ACERP: Vol. 1, No. 3, (Autumn 2015) 34-38

Advanced Ceramics Progress

Research Article

Journal Homepage: www.acerp.ir

In Vitro Evaluation of Apatite/Wollastonite Glass–ceramic Nano Biocoatings on 316 Steel Alloys by Plasma-sprayed

I.Mobasherpour*, E. Salahi, M. Razavi, A. Asjodi

Department of Ceramic, Materials and Energy Research Center, P.O. Box 31787/316, Karaj, Iran

PAPER INFO

Paper history:
Received 03 January 2013
Accepted in revised form 10 February 2014

Keywords:
Apatite
Wollastonite
Bio coatings
simulated body fluid
Plasma spraying

ABSTRACT

Among bioactive ceramics, the apatite/wollastonite (A/W) glass-ceramic, containing apatite and wollastonite crystals in the glassy matrix, has been largely studied because of high bioactivity and used in some fields of medicine, especially in orthopedics and dentistry. However, medical applications of bioceramic are limited to non-load bearing applications because of their poor mechanical properties. Apatite/wollastonite coatings on 316 steel alloys substrates were prepared by plasma spraying and incubated in simulated body fluids for different periods to investigate the nucleation and growth of apatite on their surface. The morphology and the microstructure of the coatings were observed by scanning electron microscopy (SEM) and the phase composition was examined by X-ray diffraction (XRD) and fourier transform infrared spectroscopy (FT-IR). The bioactivity of the coatings was evaluated by soaking the samples in a simulated body fluid (SBF) for 7 and 14 days. The results showed that carbonate hydroxyapatite can be formed on the surface of the coating soaked in SBF for 7 days. With longer immersion periods, the coating surface was covered by carbonate hydroxyapatite, which indicated that the apatite/wollastonite coating possesses good bioactivity.

1. INTRODUCTION

Since the discovery of bioglass by Hench et al. [1] in 1969, several glasses and glass-ceramics were found to bond to living bone [2-6]. These materials are known as bioactive ceramics: the surface is able to form a biologically active carbonate hydroxyapatite (CHA) layer which provides the bonding interface with biological tissues. The CHA phase that forms on bioactive implants is similar to the mineral phase in bone, both chemically and structurally [7, 8]. Apatite/wollastonite (A/W) glass–ceramic can form a tight chemical bond with bone and can produce a high mechanical strength, compared to other ceramics [9-12]. It is currently used in medical applications, either in powder form as bone filler or as a bulk material [13]. However, the A/W glass–ceramic, due to its relatively low fracture toughness, cannot be used in load bearing applications, such as in femoral and tibia bones. In these applications, metallic materials such as stainless steel, Co–Cr–Mo alloys and titanium alloys are used [14]. However, these materials do not directly bond to living bone [14]. The problem can potentially be solved by applying bioceramic coatings onto metal substrates. For this reason, different coating techniques have been introduced such as dip coating, electrophoretic deposition, sintering, hot isostatic pressing, flame spraying and plasma spraying [15, 16]. Plasma spraying is the most popular deposition technique due to its process feasibility as well as reasonably high coating bond strength and mechanical property [17]. Several bioactive materials, such as hydroxyapatite (HA) [18, 19] and bioglass (BG) [20, 21], have been coated on to metals and alloys substrates by plasma spraying. The object of this work was to deposit apatite/wollastonite biocoatings on 316 alloy substrate by atmospheric plasma spraying (APS) and to investigate microstructure and phase composition of coatings. The bioactivity of the coatings also was evaluated by examining carbonate hydroxyapatite formation on their surface in simulated body fluid (SBF).

2. MATERIALS AND METHOD

The glass composition reported by Kokubo et al. [9] is shown in Table 1. Frit was employed in this investigation, with the same nominal composition reported by Kokubo et al. The batch mixtures for A/W

*Corresponding Author's Email: iman.mobasherpour@gmail.com

glass–ceramic were prepared from commercial pure raw material of: SiO_2 (Merck Art No. 113126), MgO (Merck Art No. 105866), CaO (Merck Art No. 102109), P2O5 (Merck Art No. 100549) and CaF_2 (Merck Art No. 102840). The batches were placed in a alumina crucible and melted in an electric furnace at 1550 °C for 1 h. Glass powders were obtained by fritting the glass in water. The fabricated glass–ceramic frits were milled with a fast planetary moving mill, with Al_2O_3 balls and in dry conditions, with 250 rpm for 2 hours.

TABLE 1. apatite/wollastonite glass–ceramic Nominal composition in oxides (wt%).

Composition	SiO_2	CaO	P_2O_5	MgO	CaF_2
%wt	34	44.7	16.2	4.6	0.5

In order to improve the microstructure and the mechanical properties of the as-sprayed A/W coatings by sintering and crystallization, thermal treatments were performed in an electric furnace. The heating rate was 10 °C/min. On the basis of the glass transition and crystallization temperatures from STA analysis, crystallization isotherms were chosen, in order to obtain sintered and crystallized coatings, with a good microstructure. Crystallization isotherms at 900 °C for 1 h were performed on A/W powders.
Particle size distribution analysis was performed for the frit powder by the dynamic laser scattering technique using Frits ch particle sizer analysette. It can be found from Figure 1 that the particle size (D50) of the powder that was calcined at 900 °C for 60 mints was 11.27 µm, and the number percentage of the particles below 31.32µm was 90 %.

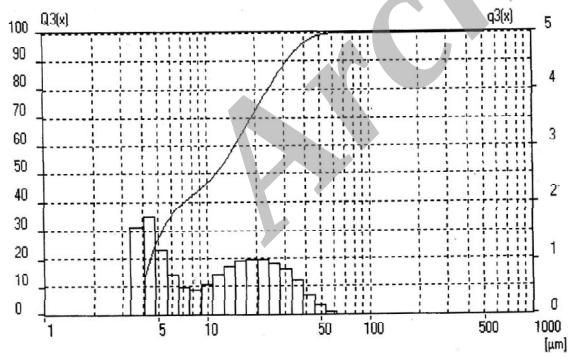

Figure 1. Particle sizes distribution of frit powder calcined at 900 °C for 60 mints.

The heat treatment A/W glass–ceramic powders were plasma-sprayed on 316 steel alloy substrates using a system equipped with a 3MB torch, in APS mode, using the operating parameters listed in table 2. The powders were characterized by means of STA analysis (Laboratories PL-STA 1640 Polymer), heated from room temperature to 1200 °C at 10 °C /min, in order to obtain the critical temperatures of the frits, such as glass transition and crystallization temperatures. The substrates of 316 steel alloys, having dimensions of 15mm×10mm×2mm, were pre-grit blasted with SiC particles before deposition.

TABLE 2. Plasma torch operating parameters.

Operating parameters	Spraying distance [mm]	Feed rate [gr/min]	Current [A]	Ar/H2 flow	Nozzle diameter [mm]
A/W coating	100	15	400	85/15	6.5

After being ultrasonically washed in acetone and rinsed in deionized water, specimens were soaked in the SBF solution whose ion concentrations nearly equal to those of the human body blood plasma [22]. The SBF solution was buffered at pH 7.4. Samples that would be analyzed by scanning electron microscopy (SEM), X-ray diffraction (XRD) and infrared spectroscopy (IR) were immersed in SBF which was renewed every day for, 7 and 14 days at 36°C without stirring.
Scanning electron microscopy (Cambridge SEM, 25Kv) was used to observe the morphologies of coatings before and after immersion. The surface of samples was sputter coated with gold for morphological observation. For cross section samples were sectioned with a low-velocity diamond saw and cross-section was cold-mounted in vacuum in epoxy resin, then polished.
The phase analysis of coatings before and after immersion was performed by using an X-ray diffractometer (XRD: Siemens, Germany), operating with Cu Kα radiation at 30 kV and 25 mA. The analyzed range of the diffraction angle (2θ) was between 20° and 70°, with a step width of 0.02°. scherrer proposed a method of deconvoluting size by looking at the peak width as a function of diffracting angle 2θ and the instrumental corrected broadening, β_{hkl}, corresponding to the diffraction peaks of apatite and wollastonite were estimated using the following equation:

$$t = k\lambda / \beta_{hkl} \cos\theta_{hkl}$$

Where k is the shape factor (0.9), ƛ is the X-ray wavelength (1.5405 Å), θ_{hkl} is the Bragg angle and t is the effective crystallite size normal to the reflecting planes. The instrumental corrected broadening, β_{hkl}, was approximated by a Gaussian fit, as full width at half-maximum (FWHM) which was calculated by using X-ray diffraction Analysis software based on each diffracting angle of 2θ. Also, X-ray diffraction Analysis software (Xpert High score plus) was used to identify the phases.

A few micrograms of the layer formed on the coating in SBF were scraped off. This was mixed with KBr and

pressed into plates for structural analysis using infrared (IR) spectroscopy on a Bruker IFS 48.

3. RESULTS & DISCUSSION

The DTA and TGA (STA) thermal analysis, reported in Figure 2, indicated that the A/W glass–ceramic has a T_g at around 780 °C. The DTA curve showed one exothermal crystallization peak (T_p), at around 845 °C. With increasing temperature from 25 to 1200 °C no weight loss in TGA graph was observed.

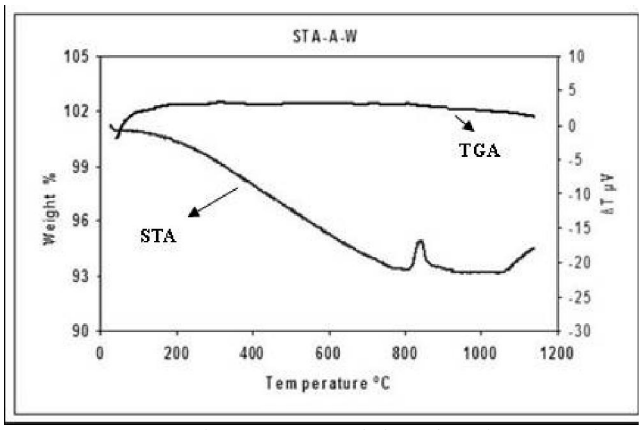

Figure 2. DTA and TGA traces of the A/W glass–ceramic powder (heating rate 10 °C/min).

Figure 3 showed SEM photographs of the surface microstructure of the as-sprayed apatite/wollastonite glass-ceramic coatings. From Figure 3, it can be seen that the coating is characterized by a rough surface, with some partially melted particles (Figure 3a). Under higher magnification, the structure of the coating appears to be highly melted and a few micro-cracks on the surface of the coating (Figure 3b).

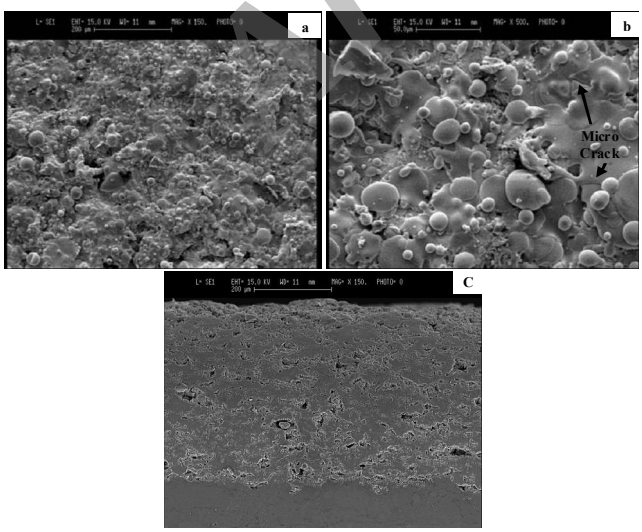

Figure 3. SEM photographs of as-sprayed A/W coatings

The cross-sectional view of the coating revealed a lamellar structure with some pores and without obvious cracks between coatings and substrate. The as-sprayed AWC coating had an average thickness of 400 μm (Figure 3c).

Figure 4 shows the XRD patterns of the apatite/wollastonite powder and coatings. From Figure 4a, it can be seen that the apatite and wollastonite phases have crystallinity. Some changes can be noted in Figure 4b, including an increase in the background area under the sharp peaks. The sharp peaks represented crystalline wollastonite and the diffuse background represented the amorphous phase. This indicated a lot of amorphous phase is present in the coating. In addition, the relative intensity of the peak at 2θ=43.58° increased manifestly comparing with Fig 4a. The observed strong peak could not be used to identify the proper crystalline phase. However, it may correspond to (311) crystal planes of wollastonite, though the intensity of this reflection in the JCPDS card is not the strongest. The phenomena may indicate that there is a probability of crystallite orientation in the plasma sprayed apatite/wollastonite coatings. Roome et al. [23] reported that crystallite orientation could be found in thermally sprayed hydroxyapatite coatings. Orientated coatings was a consequence of the thermal deposition process, where the significantly molten powders undergoes rapid recrystallization (from remaining microscopic fragments or seeds of crystalline grains) and crystal growth upon striking the substrate [23]. The apparent size of apatite and wollastonite crystallites obtained from XRD profile analysis by Scherrer method before spraying are 13 nm and 13.5 nm respectively.

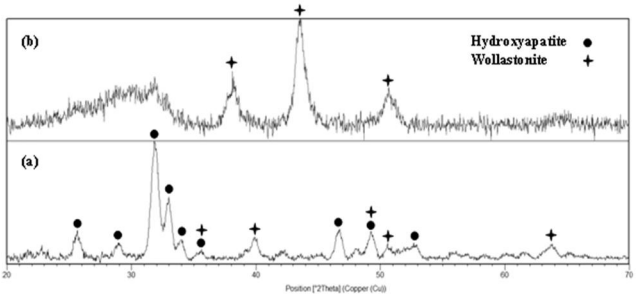

Figure 4. XRD patterns of (a) apatite/wollastonite powder and (b) as-sprayed apatite/wollastonite coating

Figure 5. shows the morphologies of the coatings immersed in SBF for various periods. From Figure 5, it can be seen that granular crystals appeared on the surface of the coating soaked in SBF for 7 days (Figure 5a). After 14 days immersion in SBF, the surface of the apatite/wollastonite coating was completely covered by the plate-like particles, which changed the original morphology of the as-sprayed coating completely (Figure 5b). With longer immersion periods, micro-

cracks similar tortoise shell character appeared on the newly formed layer. At a higher magnification, the apatite layer showed very small particles in nanometer range (Figure 5c).

Figure 6 shows the XRD patterns of the apatite/wollastonite coatings soaked in SBF solution for various times. The peak (2θ=31.7°) of carbonate hydroxyapatite (CHA) crystalline phase, could be observed in the XRD patterns of the coatings soaked in SBF solution for 7 days, and the peak was very broad resulting from super fine grains of CHA and amorphous calcium phosphate. With the increase of soaking time, the primary peak (2θ=31.7°) of the crystalline CHA became higher in intensity and the secondary strong peak (2θ=33°) of the crystalline CHA can be seen from Figure 6b.

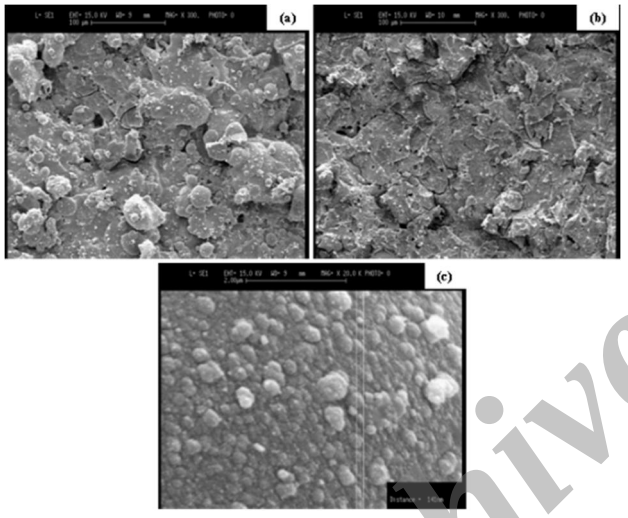

Figure 5. Surface morphologies of apatite/wollastonite coatings after immersion in SBF for various periods: (a) 7 d; (b) 14 d; (c) higher magnification for carbonate apatite layer.

These are attributed to the transition of amorphous calcium phosphate to a crystalline phase and the growth of crystalline CHA grains by taking calcium and phosphate ions from the SBF solution.

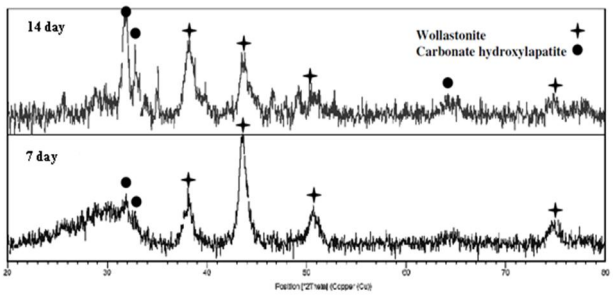

Figure 6. XRD patterns of apatite/wollastonite coatings soaked in SBF for various periods.

Figure 7 shows the FT-IR spectra of the surface layer of the coating immersed in SBF for 14 days. The FT-IR spectrum of the coatings soaked in SBF for 14 days showed that the carbonate hydroxyapatite (CHA) appeared on the surface of the coatings. Bands at 604 and 563cm^{-1} are due to the bending vibration modes of the PO_4^{3-} group. A very broad OH^- absorption bands from 3800 to 3200 cm^{-1} can be seen in these spectra. Band around 707 cm^{-1} is due to the carbonate FTIR absorption. The broad bands around 1045cm^{-1} is mainly attributed to the phosphate FTIR absorption. The peak around 494 cm^{-1} is attributed the silicate (O-Si-O) FTIR absorption. The formation of carbonate hydroxyapatite (CHA) on the surfaces of plasma sprayed apatite/wollastonite coatings is similar to that of CaO-SiO_2-based glasses.

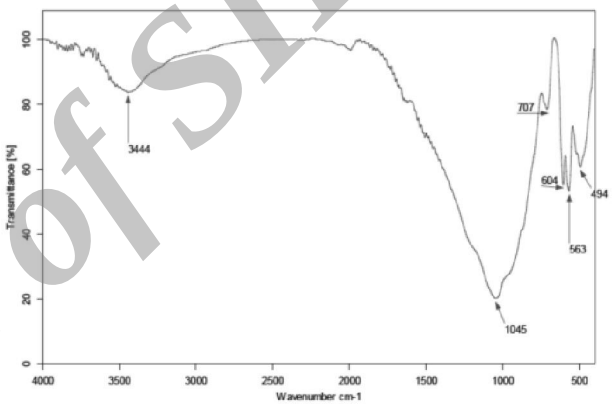

Figure 7. FT-IR spectra of the apatite/wollastonite coatings soaked in SBF for 14 day.

The calcium ion dissolved from the apatite/wollastonite coatings increase the ion activity product of the apatite in the SBF solution, and the hydrated silica on the surfaces of the apatite/wollastonite coatings provides favorable sites for apatite nucleation. Consequently, the apatite nuclei are rapidly formed on the surface of the apatite/wollastonite coatings. Once the apatite nuclei are formed, they spontaneously grow by consuming calcium and phosphate ions from the SBF solution. The calcium phosphate phase that accumulates on the surface of the apatite/wollastonite coatings is initially amorphous. It later crystallizes to a hydroxycarbonate apatite (HCA) structure by incorporating carbonate anions from solution within the amorphous calcium phosphate phase [1].

4. CONCLUSION

Apatite/Wollastonite coatings on 316 steel alloys substrates were prepared by plasma spraying. The structure of the coating appears to be highly melted and a few micro-cracks on the surface of the coating .The

crystalline wollastonite which may be preferred orientation and the amorphous phase can be found in the coatings. The carbonate hydroxyapatite (CHA) was formed on the surface of the coatings soaked in SBF for 7 days. With longer immersion periods, the surface of coatings was covered by dense carbonate hydroxyapatite; therefore, the plasma-sprayed apatite/wollastonite coatings possess the potential for excellent bioactivity and thus may be used as a candidate of biomaterials.

ACKNOWLEDGMENTS

The authors would like to acknowledge the financial support of Materials & Energy Research Center of Iran for this research.

REFERENCES

1. Hench L.L, Anderson O, Bioactive glass. In: Hench LL, Wilson J, editors. USA: ***World Scientific***; (1993), 41–62.
2. Kokubo T, A/W glass-ceram ic: processing and properties. In: Hench L.L, Wilson J, editors, USA: ***World Scientific***; (1993), 75–88.
3. LeGeros R.Z, LeGeros JP. Dense hydroxyapatite, In: Hench LL, Wilson J, editors. USA: ***World Scientific***; (1993), 139–80.
4. Hench L.L, ***Journal of the American Ceramic Society***, Vol.74 (1991),1487–510.
5. Hench L.L, ***Journal of the American Ceramic Society***, Vol. 81, (1998) , 1705–28.
6. Kokubo T, Kim HM, Kawashita M, ***Biomaterials***, Vol. 24, (2003), 2161–75.
7. Kokubo T, Ito S, Huang T, Hayashi T, Sakka S, and Kitsugi T, ***Journal of Biomedical Materials Research***, Vol. 24, (1990), 331–343.
8. Ratner B.D, Hoffman A.S, Schoen F.J and Lemons J.E, Biomaterials Science, An Introduction to Materials in Medicine. ***Elsevier Academic Press***, (2004).
9. Kokubo T, Ito S, Sakka S, and Yamamuro T, ***Journal of Materials Science*****,** Vol. 21, (1986), 536–540.
10. Yoshi S, Kakutani Y, Yamamuro T, Nakamura T, Kitsugi T, Oka M, Kokubo T, and Takagi M, ***Journal of Biomedical Materials Research*****,** Vol. 22, (1988), 327–338.
11. Park J, and Ozturk A, ***Materials Letters*****,** Vol. 61, (2006), 1916–1921.
12. Kamitakara M, Ohtsuki C, Inada H, Tanihara M, and Miyazaki T, ***Acta Biomaterialia***, Vol. 2, (2006), 467–471.
13. Kokubo T, ***Biomaterials***, Vol. 12, (1991), 155–163.
14. Rack H.J, and Qazi J.I, ***Materials Science and Engineering C*****,** Vol. 26, (2006), 1269–1277.
15. Sun L, Berndt C.C, Gross K.A, and Kucuk A, ***Journal of Biomedical Materials Research***, Vol. 58, (2001), 570–592.
16. Zhao Y, Chen C, and Wang D, ***Surface Review and Letters***, Vol. 12(4), (2005), 505–513.
17. Nejati M, Rahimipour M.R, Mobasherpour I, ***Ceramics International*****,** Vol. 40, (2014), 4579–4590.
18. Nimkerdphol A.R, Otsuka Y, Mutoh Y, ***Journal of the Mechanical Behavior of Biomedical Materials***,Vol. 36, (2014), 98-108.
19. Vuoristo P, ***Comprehensive Materials Processing***, Vol. 4, (2014), 229-276.
20. Singh G, Singh H, Singh Sidhu B, ***Surface and Coatings Technology*****,** Vol. 228, (2013), 242-247.
21. Demnati I, Grossin D, Errassifi F, Combes C, Rey C, Le Bolay N, ***Powder Technology***, Vol. 255, (2014), 23-28.
22. Cho S.B, Nakanishi K, Kokubo T, Soga N, ***Journal of the American Ceramic Society***, Vol. 78, (1995), 1769-1774.
23. Roome C.M, Adam C.D, ***Biomaterials,*** Vol. 16, (1995), 691-696.